Time-of-Flight (ToF) Cameras for Underwater Situational Awareness

Kevin V. Mack*, William D. Jemison*, Luke K. Rumbaugh*, David W. Illig†, Mahesh K. Banavar*

*Department of Electrical and Computer Engineering
Clarkson University, Potsdam, NY 13699.
{mackkv, wjemison, lrumbaug, mbanavar}@clarkson.edu

†Electro-Optics and Special Missions Sensor Division, NAWCAD
Patuxent River, MD 20670
david.w.illig@navy.mil

Abstract—Recently developed commercial Time-of-Flight (ToF) cameras have been used to accurately and reliably measure scene depth with high resolution in applications such as automotive LiDAR. There is a desire to adapt this technology for applications in underwater environments. In this work, we establish a methodology for using modified commercial ToF cameras in turbid water. We express the need for hardware and software modifications to the camera and demonstrate initial results in the efficacy of the camera in an underwater test scenario. We include ToF camera imagery taken under a variety of water conditions to understand the performance limitations of this technology as a function of water clarity. Target detection results from preliminary laboratory test tank experiments are presented for two different classifiers, each of which achieves high accuracy for a certain range of water conditions.

Index Terms—Time-of-Flight Camera, ToF, Ranging, Underwater, Turbid

I. INTRODUCTION

Laser-based sensors offer the potential for high-resolution 3D imaging in the underwater environment. Most approaches require scanning the laser transmitter, optical receiver, or both in order to build a full 3D image one pixel at a time [1]. On the other hand, commercial-off-the-shelf (COTS) ToF cameras use a flash illuminator and specially designed optical receivers to simultaneously image an entire 3D volume. We believe this technology will continue to be developed by the automotive industry [2], and can be leveraged for underwater imaging applications. The rest of this paper describes challenges of adapting COTS ToF cameras for use underwater, a proof-of-concept setup and initial results, and our future work plans.

II. TECHNICAL CHALLENGES AND METHODOLOGY

There are two main challenges when attempting to use an optical sensor in a turbid water environment: absorption and scattering [3]. The first challenge also represents a hardware issue with COTS ToF cameras, due to their use of infrared (IR) or near IR (NIR) modulated light to perform ranging. The second challenge is related to the increased collection of scattered light in comparison to operation in air.

A. Absorption of IR Light By Water

The first challenge in adapting COTS ToF camera for underwater use is the physics of absorption of electromagnetic waves by water. Water strongly absorbs the region of the spectrum corresponding to IR light (700 nm - 1 mm) [3]. In order to operate at practical standoff distances, the ToF illuminator must use a frequency of light that has a lower absorption coefficient than the IR/NIR band. In particular, water absorption is minimized in the blue-green band (400-500 nm) [4]. This means that to adapt a COTS ToF camera for use underwater, several hardware modifications are required to enable use with blue-green rather than IR/NIR light. For this work we have selected the ESPROS epc660 ToF camera, in large part due to its modularity. Adapting this camera required two steps. First, the receiver was modified by removing a NIR bandpass filter. The second modification was to create a green illumination source. A benchtop setup was constructed to test these hardware modifications and is shown in Figure 1.
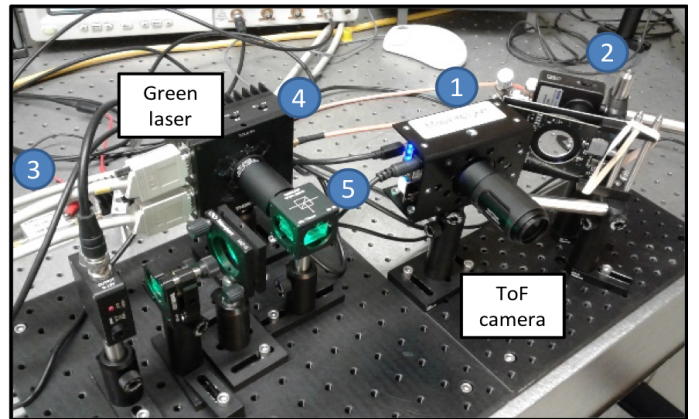

Fig. 1. The benchtop setup for the ToF camera with green laser diode illuminator. The labels in the image represent 1. ToF Camera, 2. NIR illuminator and photodetector, 3. amplifier, 4. laser diode modulation fixture, and 5. green laser diode output

In our first hardware iteration, to guarantee that the modulation waveform is phase-locked to the ToF camera's receiver hardware, the original NIR output waveform was detected and

used to drive a green laser diode illuminator. We verified that the green laser light matched the original NIR modulation, as given by Figure 2. Future work will aim to phase lock the green illuminator module directly to the ToF camera.
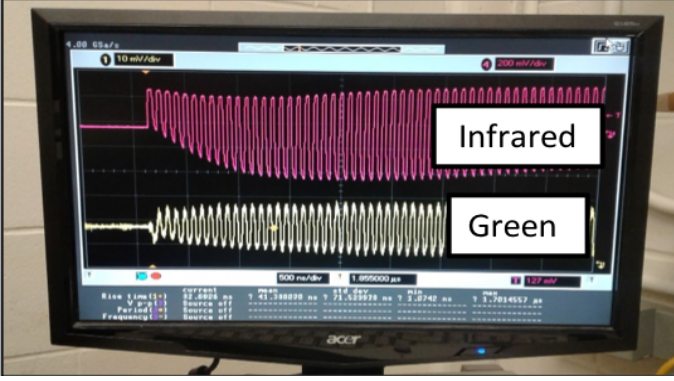

Fig. 2. An example of an intensity modulated signal sent out by the ToF camera. The signal is collected from the output of the illuminator into a photodetector and displayed on an oscilloscope. The graph on top is the original infrared signal, the graph on the bottom is the copied version for the green laser diode.

We performed a test in a small water tank in order to demonstrate the ToF camera's functionality with the green illuminator. Figure 3 depicts a baseline test with the NIR illuminator and a post-modification test with the green laser diode illuminator. Along the top row it can be seen that while the NIR illuminator produces a good image in air, it produces an image with an almost complete lack of contrast in water, as expected due to absorption of NIR radiation by the water. The images along the bottom row show a test through water with the green illuminator, showing that the ToF camera has the ability to produce useful images of the target object.
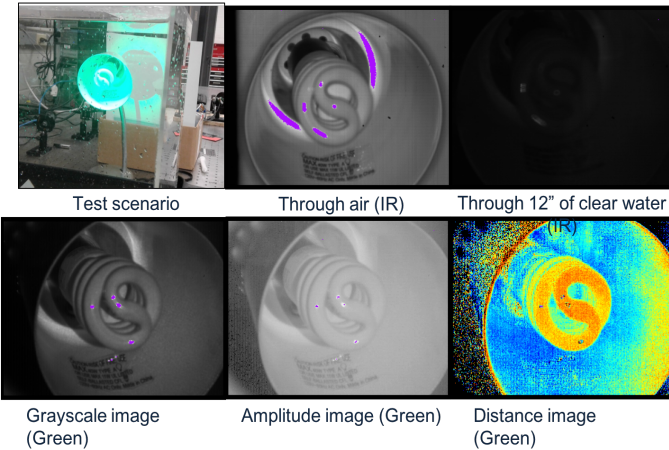

Fig. 3. The test scenario uses a small water tank with a desk lamp as the target object. One set of images was taken with the NIR illuminator and compared to the in air image. Then a set of images was taken with the green laser diode, and shows an improved ability to detect the target in water.

B. Light Scattering

In turbid waters, due to water particles and particulates suspended in the water itself, much of the light emitted from an optical transmitter is reflected back to the detector before it reaches the target object [5]. This phenomena is known as backscatter, essentially a "clutter" signal that causes erroneous range measurements. This effect is especially present in turbid water, and is the focus of much work that attempts to improve underwater rangefinding. A second type of scattering is forward scatter, which causes beam-spreading and results in blurring of image features. An example of backscatter and forward scatter in a LiDAR signal is given by Figure 4. We will characterize the effects of backscatter on our modified ToF camera, which will then motivate processing techniques to reduce that scatter signal.
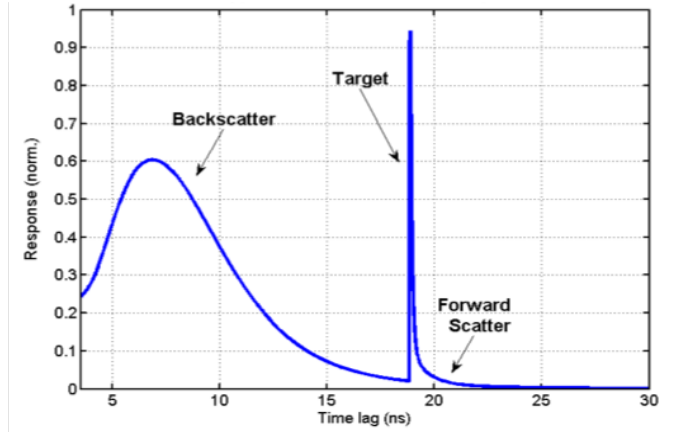

Fig. 4. An example of the return from a LiDAR ranging signal. The different components of the return signal are the backscatter, the target return, and the forward scatter.

C. Data Acquisition and Processing

The ESPROS epc660 camera has essentially two main modes of operation, grayscale and distance mode, which correspond to whether or not the transmitted light is modulated. In grayscale mode, the ToF camera essentially functions as a traditional camera. The result is a grayscale image with no depth information and no ambient light suppression (no modulated light is used). In distance mode, the camera leverages its ability to emit modulated flash illumination and reject ambient light. The raw data received, known as differential correlation sample (DCS) data, can be used to create a depth image or an amplitude image by processing the DCS data.

The ToF camera operational principles that allow for ranging estimates to be made in air still apply in the underwater scenario. The ESPROS epc660 imager is able to detect the pulsed sinusoidal modulation signal by making differential correlation sample (DCS) measurements at each pixel in the pixel field. The ToF camera performs four successive DCS frame acquisitions $(DCS_0, DCS_1, DCS_2, DCS_3)$ for each distance measurement. Each DCS frame applies two demodulation signals to the return signal, and provides the camera with

two truly unique DCS measurements and two redundancies. These redundancies are included to help compensate for fixed pattern noise and device mismatches in hardware during the pixel readout. The demodulated signals are then integrated over one full period, and following their differences are computed to obtain the DCS samples. The significance of taking the difference is to suppress ambient, unmodulated light. Given four DCS sample measurements and a calibration offset, the range is given by,

$$D = \frac{\nu}{2} \cdot \frac{1}{2\pi f_{mod}} \left[\pi + atan \left(\frac{DCS_2 - DCS_0}{DCS_3 - DCS_1} \right) \right] + D_{offset},$$
(1)

where ν is the speed of light in the medium, f_{mod} is the modulation frequency, and D_{offset} is the offset distance from a calibration step. From the structure of (1), it is apparent that the DCS measurements have some relation to the concept of in-phase/quadrature (IQ) samples from radar signal processing. With (1) and some further analysis, it can be shown that the previous range equation is equivalent to

$$D = \frac{\nu}{2} \cdot \frac{1}{2\pi f_{mod}} \left[\pi + \phi(obj) \right] + D_{offset},$$
(2)

This form is similar to the standard range calculation used with sinusoidal modulation and IQ demodulation with the presence of some constant offset factors. It can also be shown that in this context $DCS_0 = -DCS_2 = TQ$, and $DCS_1 = -DCS_3 = -TI$, where T refers to the period of the modulation signal.

III. EXPERIMENTS

To test the ToF camera operation in a turbid underwater scenario, an experiment was performed in a 100 liter fish tank with the hardware setup described in previous sections. The dataset will be examined and used to train a classifier for target detection, as well as characterize the camera performance in various levels of water turbidity, as measured by a C-Star transmissometer (Sea-Bird Scientific).

A. Experimental Setup

The experimental setup includes the benchtop setup mentioned in Section II with the 532nm laser aimed into a 100 liter fish tank. The ESPROS ToF camera features a telescopic lens with an optical wavelength filter that is matched to the laser. A 24 MHz sinusoidal modulation signal was produced by the camera to modulate the laser and illuminate the target, which was positioned 70 cm away from the camera. This setup is depicted by Figure 6. Submerged in the tank is a diffuse target made of LEGO® bricks roughly 25 cubic cm in size (depicted in Figure 5).

The dataset is summarized in Table I, which includes both the measured beam attenuation coefficient c and the number of optical attenuation lengths downrange to the target. The attenuation length is a unitless parameter obtained by multiplying c by the distance downrange to the target. This metric is useful for extrapolating the test conditions to different ranges and/or different water conditions.

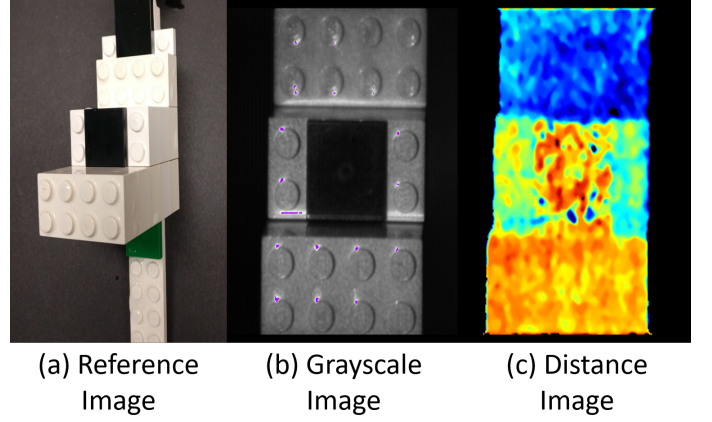(a) Reference Image (b) Grayscale Image (c) Distance Image

Fig. 5. Images of the target object from our dataset. The object is made of LEGO® bricks and provides a 3D diffuse target for underwater imaging. Image (a) is a reference image of the object taken with a cellphone camera against a black backdrop, (b) is a grayscale image taken with the ToF camera through clear water, and (c) is a distance image taken with the ToF camera in clear water. The distance image is a false color image, with the color representing the depth of the scene.
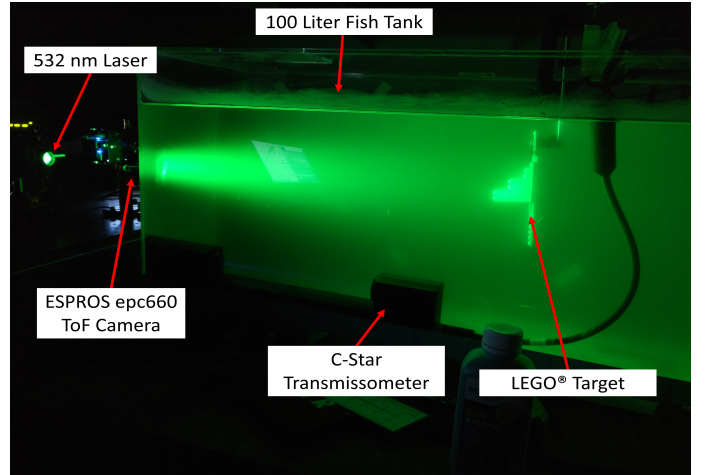

Fig. 6. Photograph of the test setup described in Section III. Portions of the image are labeled, such as the 532 nm laser, the ESPROS epc660 camera, the C-star transmissometer, the LEGO® target, and the fish tank.

Turbidity Level	Measured c (m^{-1})	Attenuation Lengths
T0	1.233	0.740
T1	3.128	1.877
T2	4.548	2.729
T3	6.113	3.668
T4	7.658	4.595
T5	8.956	5.373
T6	11.653	6.992
T7	14.355	8.613
T8	19.521	11.712
T9	24.972	14.983

TABLE I
EXPERIMENT PARAMETERS

IV. ANALYSIS AND RESULTS

To characterize the performance of the camera in the experimental setup, we first compare the dataset to theoretical

calculations from Beer's Law for light attenuation through a material. The idea is to track how the amplitude of the target return decreases as attenuation length increases, in order to validate the experimental setup against theoretical behavior. We also present some preliminary results for target detection in various levels of turbidity. Once again, the dataset described in Section III-A will be used for this task. We compare results from a linear classifier and a multilayer perceptron.

A. Target Return in Turbid Water

In accordance with Beer's law, the intensity of light decreases exponentially with respect to attenuation lengths. This relationship is given by,

$$P = P_0 e^{-cz}, \tag{3}$$

where P_0 is the transmit power, c is the turbidity, and z is the distance [3]. We take the average amplitude of the target return in clear water to be our transmit power, P_0, our distance is constant at $z = 70$ cm, and our turbidity c are the measured values given in Table I.

To find the average target amplitude, we extract the target pixels with a well known image thresholding method called Otsu's method [6]. Otsu's method parses foreground pixels from background pixels: in this case the foreground will be our target object. We use this thresholding method on amplitude data for each turbidity level, extracting the average target amplitude for each turbidity. Examples of the thresholding results are given in Figure 7 for three turbidities. Due to an issue in the experimental setup, the target position varies slightly within the image frame between turbidities. In Figure 7, false-color amplitude images are plotted on the left, with the other columns showing how the thresholds are determined and applied. The right column shows the amplitude histograms, built by counting the number of times each discrete amplitude value appeared in the images. Otsu's method is applied to these histograms to determine an amplitude threshold to separate target pixels from non-target pixels. The center column shows the result of applying this threshold, with pixels classified as belonging to the target shown in white and non-target pixels shown in black. As the turbidity increases, image contrast is lost which reduces the discrimination of Otsu's method, as can be seen for example for T7.

Measured and theoretical target amplitude results are given in Figure 8. The measured results were obtained using Otsu's method as described above. The theoretical values were obtained by measuring the target amplitude in clean water and then applying Beer's Law to the turbidity values used in the experiment. It should be noted that the actual target amplitude in Figure 8 is greater than the theoretical prediction of Beer's Law: this is to be expected as Beer's Law assumes all scattered light is lost, when in fact some scattered light is collected by the receiver. With this caveat in mind, the measured and theoretical results show good agreement, verifying that the ToF camera sensor is behaving as expected for underwater imaging. This type of analysis may be used in future experiments to

estimate at what turbidity the target-to-backscatter ratio will fall below a desired threshold.
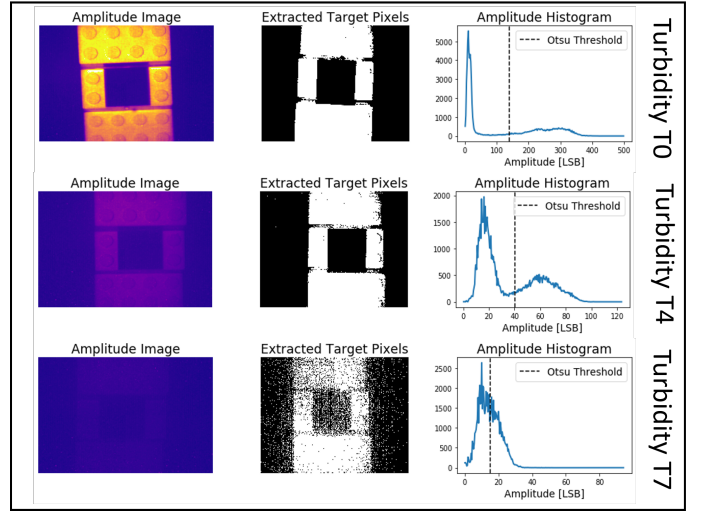

Fig. 7. Otsu's method for image thresholding is used to seperate the target pixels from the background. This method is effective for most cases, even when attenuation length is relatively high.
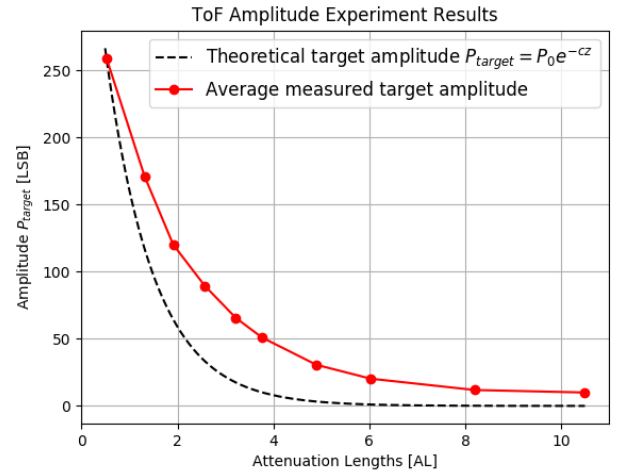

Fig. 8. Results of Beer's Law target amplitude test. The target amplitude measurements show good agreement with the theoretical predictions.

B. Target Detection

With the dataset described in Section III, it is possible to test a target detection algorithm. The idea is to classify each image as having a target in the field of view, or no target present. This would be a useful pre-processing step for future processing chains. While this dataset is not generalized to different targets and distances, it can still inform us of detection performance in differing turbidity levels. The results can be used in further work, with more generalized data, to define which classifiers may perform well in future experiments. Figure 9 gives example amplitude images from the dataset in varying levels of turbidity. The figure also shows how the

backscatter noise increases in amplitude as turbidity increases. This is represented by images with no target present, thus all received power should be attributed to backscatter. It should be noted that in the T0 image, i.e. clear water, a reflection from the back of the tank saturates part of the image.

(a) Amplitude Image Backscatter Only   (b) Grayscale Image Target Present   (c) Amplitude Image Target + Backscatter
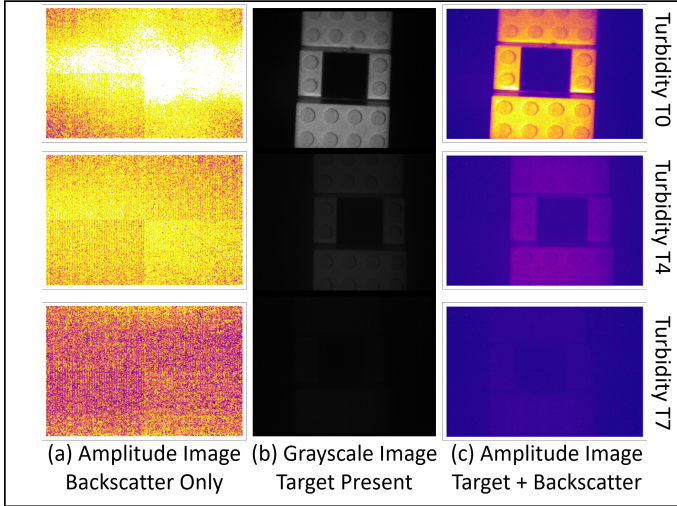
Fig. 9. Example of data collected during the experiments described in Section III. The figures in column (a) show the amplitude of the backscatter (with no target present) for various turbidity levels. At turbidity T0, the saturated portion in the middle of the image is a reflection off the back of the fish tank. Column (b) are grayscale images taken at select turbidities with a target object in view, and column (c) are the amplitude images for column (b). In column (a), the T0 turbidity case has a saturated portion at the center of the image, which is the result of a reflection from the back window pane of the fish tank. This effect is not present in the other higher turbidity cases because the return from the back of the tank was highly attenuated.

The results of target detection in turbid water are given by Table II. The table compares results from a linear support vector machine (SVM) which was trained on image variance, and a multilayer perceptron (MLP) with two hidden layers and the amplitude image as input. Currently, the detection algorithms are tested only on amplitude data, however in future work we aim to utilize raw DCS and distance data for comparison. The current implementation uses test and train data taken at a single distance, turbidity, and modulation frequency with only the target pictured in Figure 5. We note from Table II that detection accuracy begins to roll-off starting at T7, which matches the qualitative results seen plotted in Figure 7 and Figure 9. However it should also be noted that the high detection accuracy is potentially due to over-fitting on a dataset that lacks diverse features and should not be generalized to other datasets at this time. Future work will look to test our target detection on more diversified features, adding multiple distances, target objects, and modulation frequencies.

V. Conclusions

Commercial ToF cameras are known to be cost effective, reliable, and compact instruments for ranging and 3D imaging when operating in air. These capabilities would benefit a variety of underwater sensing applications as well. In this work, we demonstrated a proof-of-concept system that allows

Turbidity Level	Variance SVM	MLP Network
T0	100 %	100 %
T1	100 %	100 %
T2	100 %	100 %
T3	100 %	100 %
T4	100 %	100 %
T5	99 %	100 %
T6	98 %	99 %
T7	93 %	98 %
T8	68 %	83 %
T9	50 %	63 %

TABLE II
Target Detection Results

us to take 3D depth images through water in a laboratory environment. Of the two technical challenges described in Section II, the hardware challenges related to absorption have been addressed. We are now capable of collecting ToF camera imagery, and this has been demonstrated by taking a variety of images across water clarities. We have also demonstrated a target detection scheme that can potentially aid in later work with underwater ranging.

Future work will aim to enhance the hardware of our modified ToF camera, such as increasing optical power. With greater optical power, we can test performance under conditions that are more representative of large volumes of water. In further experiments, we aim to provide a more generalized dataset for target detection, varying not just water clarity, but distance, modulation frequency, and target shape as well. We then intend to investigate processing techniques to reduce the effects of scattered light on system ranging performance.

Acknowledgments

References

[1] Dalgleish, F.R. et al., "Extended-Range Undersea Laser Imaging: Current Research Status and a Glimpse at Future Technologies", Marine Technology Society Journal 47(5):128-147 (2013).
[2] Hecht, J., "Lidar for Self-Driving Cars", Optics & Photonics News 29(1):26-33 (2018).
[3] Mobley, C.D., "Light and Water", Elsevier Science, San Diego (1994).
[4] Smith, R., and Baker, K., "Optical properties of the clearest natural waters", Applied Optics 20(2):177-184 (1981).
[5] Mullen, L.J. and Contarino, V.M., "Hybrid lidar-radar: seeing through the scatter", IEEE Microwave Magazine 1(3):42-48 (2000).
[6] Otsu, N., "A threshold selection method from gray-level histograms", IEEE Trans. Sys. Man. Cyber. 9(1):62-66 (1979).